Article

# Measurement of Double-Layer Forces at the Electrode/Electrolyte Interface Using the Atomic Force Microscope: Potential and Anion Dependent Interactions

Andrew C. Hillier, Sunghyun Kim, and Allen J. Bard

*J. Phys. Chem.*, **1996**, 100 (48), 18808-18817 • DOI: 10.1021/jp961629k

# Measurement of Double-Layer Forces at the Electrode/Electrolyte Interface Using the Atomic Force Microscope: Potential and Anion Dependent Interactions

**Andrew C. Hillier,[†] Sunghyun Kim,[‡] and Allen J. Bard***

*Department of Chemistry and Biochemistry, The University of Texas at Austin, Austin, Texas 78712*

*Received: June 4, 1996; In Final Form: August 8, 1996*[⊗]

The forces between a silica probe and silica and gold substrates were measured with an atomic force microscope in the presence of a series of alkali-halide electrolyte solutions. The interaction between two silica surfaces was repulsive and could be accurately predicted by Derjaguin−Landau−Verwey−Overbeek theory. The silica surface was negatively charged at a pH of 5.5 and the effective surface potential increased in magnitude with decreasing electrolyte concentration. In contrast, the force between the silica probe and a gold substrate was attractive at open circuit. This interaction was a strong function of the potential applied to the gold and the nature of the electrolyte species. In general, the silica−gold interaction changed from attractive, when the gold was held at positive potentials, to repulsive at negative potentials. A series of force measurements as a function of the potential of the gold electrode indicated that the repulsive force increased when moving toward more negative potentials, corresponding to the removal of adsorbed anions. The potential at which the silica−gold interaction passed through a minimum, referred to as the potential of zero force (pzf), corresponded closely to the potential of zero charge (pzc) in these systems. The pzf values were compared to those determined from measurements of the electrode capacitance in $10^{-3}$ M solutions of NaF, KCl, KBr, and KI. The force data were also compared to theoretical predictions of the forces between dissimilarly charged surfaces obtained by solving the complete nonlinear Poisson−Boltzmann equation.

## Introduction

Double-layer phenomena play a crucial role in interfacial systems ranging from the stability of colloids to ion partitioning at biological membranes and form the basis of electrochemical processes. Although considerable advances have been made in our understanding of the influence of double layers on physical and chemical systems,[1] direct measurement of the structure and forces residing at this interface, particularly at electrode surfaces, has been limited. We describe here how the diffuse double layer at an electrode surface can be probed at nanometer resolution with a modified tip on a cantilever of an atomic force microscope (AFM). The surface charge and potential on the electrode can be determined from the force between the electrode and the tip on the AFM cantilever.

Early attempts to measure interaction forces at solid surfaces provided some insight into double-layer phenomena.[2] Advent of the surface forces apparatus (SFA) marked a considerable advance in this area as it allowed the direct measurement of surface forces with high precision and control.[3] Due to experimental constraints, the SFA has been used primarily to measure forces between mica surfaces[3a,4] and materials adsorbed on mica (e.g., polymers[5] and molecular liquids[6,7]). However, recent design improvements[8,9] have allowed the examination of more diverse substrates, including silica.[10]

The AFM,[11] which is related to both the SFA and the scanning tunneling microscope,[12] has recently been employed to measure surface forces. The utility of this technique is the ability to examine interactions between a large variety of surfaces without regard to size, structure, or optical clarity. Double-layer forces have been examined with the AFM on a number of systems of interest to colloid chemists[13,14] and also in electrochemically relevant systems, including anion adsorption on gold[15] and the interaction between $Si_3N_4$ and gold on Langmuir−Blodgett-covered surfaces.[16] The AFM has also been used to measure local compliance,[17] surface contact potentials,[18] and adhesion between surfaces.[19] Recent advances in AFM force measurement techniques employ active force probes, including the rocking beam force balance[20] and the interfacial force microscope.[21] These now allow sampling of near field forces within the snap-in region of passive cantilever probes (typically ≤5−10 nm).

Although force measurements in electrochemical systems have been somewhat limited, an early examination of the force between two metal wires in an eletrolyte solution illustrated a potential-dependent repulsive force.[2] More recent studies in electrochemical systems include the examination of thin-layer cell behavior[22] and electrostatic forces[7b,23] between two platinum-coated mica surfaces with the SFA and a study of surface stress at gold and platinum-coated AFM cantilever electrodes.[24] The latter study suggested a means of measuring the potential of zero charge (pzc) at an electrode by determining the potential corresponding to a minimum in surface stress, which is reminiscent of earlier work,[25] but benefits from a significantly higher sensitivity to stress at the electrode surface, compared, for example, to piezoelectric transducers attached to the electrode.[26]

The nature of the double layer in electrochemical systems is reasonably well understood.[27−29] Typically, changes in the diffuse double layer produce a charging current with a change in electrode potential. Surface tension or electrocapillary measurements at liquid (Hg) electrodes[28a,30] and capacitance studies[31] at liquid and metal electrodes have provided considerable experimental insight into the surface charge and double-layer composition. We describe here how the diffuse double layer (dl) at an electrode surface can be probed at nanometer resolution with an AFM. The dl is examined by measuring the force between a spherical probe tip placed on the end of an

[†] Current address: Department of Chemical Engineering, University of Virginia, Charlottesville, VA 22903.

[‡] Current address: Department of Chemistry, Konkuk University, Seoul, Korea 133-701.

[⊗] Abstract published in *Advance ACS Abstracts,* November 1, 1996.

S0022-3654(96)01629-2 CCC: $12.00 

AFM cantilever and an electrode as the probe moves through the dl. The surface charge on the electrode is inferred from the force between the electrode and the tip on the AFM cantilever as a function of the electrode potential. The influence of electrode potential on the force−distance curves between a silica probe and a gold electrode surface are examined in aqueous solutions of several 1:1 alkali-halide electrolytes, including NaF, KCl, KBr, and KI.

## Experimental Section

**Materials.** *(a) Reagents.* Solutions of NaF, KCl, KBr, and KI were prepared from reagent grade chemicals (Aldrich, Milwaukee, WI) without further purification in 18 MΩ deionized water (Milli-Q Plus, Millipore Corp., Bedford, WA). The solutions were deaerated with nitrogen for 15 min immediately before use. Typically, the pH ≈ 5.5.

*(b) Probe Preparation.* Force measurements were acquired with a microfabricated cantilever having a spherical probe tip. The spherical AFM probe was prepared in a fashion similar to the procedure of Ducker, Senden, and Pashley.[13a] Force measurements using standard cantilevers with integrated, square-pyramidal tips showed behavior similar to that seen with the spherical probe but suffered from an ill-defined interaction radius and a much smaller signal-to-noise ratio, typically 10−50 times less. A silica sphere with nominal diameter of 10−20 $\mu$m (Polysciences, Warrington, PA) was attached to the tip of a commercially available AFM cantilever (Nanoprobe, Park Scientific, Mountain View, CA) using epoxy resin (Epon 1002, Shell, Houston, TX). In a modification to Ducker's technique, an optical microscope (Olympus, Model BHTU, Tokyo, Japan) with a three-dimensional micropositioning stage was used to position epoxy and then a silica sphere near the apex of the AFM cantilever tip, while the cantilever was kept at a temperature sufficient to melt the epoxy. A soldering iron with a metal clip attachment was used to hold the AFM tip at elevated temperatures. With the tip in focus under the microscope objective, solid resin, previously melted onto a glass slide, could be positioned at the very tip of the cantilever using the micropositioning stage. The resin would melt only at the location where it touched the heated cantilever tip. With a small droplet of molten resin, a silica sphere could then be attached to the tip in a reproducible and controlled manner by bringing a glass slide covered with spheres up to the tip with the micropositioning stage. The resin solidified following removal of the heat source. In cases where the sphere adhered to off-center positions on the cantilever, a brief annealing treatment served to melt the resin and realign the sphere to the tip apex via surface tension. Immediately prior to use, the spherical probe tip was rinsed with ethanol, rinsed with purified water, and then blown dry with nitrogen. Harsher cleaning procedures (e.g., $H_2SO_4$, chromic acid, steam treatment) damaged the resin and severed the tip−probe bond.

*(c) Substrate Preparation.* Silica substrates were prepared from commercial glass cover slips that were cleaned in a concentrated sulfuric/nitric acid solution prior to exposure to condensing steam vapor for 15 min. AFM imaging of the silica surfaces indicated a mean roughness of 1.25 nm/$\mu$m$^2$ with a maximum peak to valley height of 4.2 nm over a 1 $\mu$m × 1 $\mu$m area. Gold substrate electrodes were prepared by melting high purity gold (99.99+%, Goodfellow metals) in a 1-mm-diameter hole in a 12-mm-diameter × 4-mm-thick quartz disk. Electrical contact was then made with an insulated copper wire to the gold electrode through the back side of the quartz disk with conductive epoxy (H2OS, Epotek). The quartz assembly was mounted to a magnetic, stainless steel sample disk with epoxy (Torr Seal, Varian). The gold/quartz surface was ground to optical smoothness with successively finer grades of diamond paste (15, 6, and 3 $\mu$m) and silica slurry (1, 0.3, and 0.05 $\mu$m; Buehler, Lake Bluff, IL). The polished gold surface appeared smooth by observation with an optical microscope, had an electrochemically active area of $1.96 \times 10^{-3}$ cm$^2$, and exhibited a mean roughness of 2.65 nm/$\mu$m$^2$ with a maximum peak-to-valley height of 8.2 nm over a 1 $\mu$m × 1 $\mu$m area. Prior to use, the gold electrode was sonicated for 15 min to remove any remaining silica polishing particles, followed by a 10 min rinse in hot chromic acid. Immediately prior to use, all surfaces were rinsed in EtOH, rinsed with copious amounts of purified water, and blown dry under nitrogen.

**Electrochemistry and Force Measurements with AFM.** *(a) Equipment.* Force measurements were performed with a Nanoscope III atomic force microscope (Digital Instruments, Santa Barbara, CA) equipped with probes (Nanoprobe, Park Scientific, Sunnyvale, CA) consisting of triangular silicon nitride cantilevers with integrated pyramidal tips. The probes were modified by the attachment of a spherical silica bead as described earlier. The AFM was equipped with a piezo scanner having a maximum scan range of 15 $\mu$m × 15 $\mu$m × 2 $\mu$m. Scanner calibration was achieved in the *x* and *y* directions using a 1 × 1 mm grid of gold on silicon. The *z* direction was calibrated by measuring the wavelength of the optical interference patterns resulting from reflection between the tip and a reflective substrate. This method is similar to that described by Jaschke and Butt.[32]

Solution measurements were carried out in a fluid cell (Digital Instruments) with Teflon tubing (Figure 1a). All fluid cell components were cleaned immediately before use by an extensive soak in purified water and subsequent rinse in EtOH, rinse with copious amounts of purified water, and dry under nitrogen. A three-electrode design was employed for electrochemical measurements with the Au substrate acting as working electrode, a Pt counter electrode (CE), and a SCE reference electrode (RE). The counter and reference electrodes were placed in a saturated KCl solution, which was connected through a salt bridge to the outlet port of the fluid cell. All electrode potentials are cited with respect to this SCE reference. Electrochemical control of the cell was effected with a PAR 173 potentiostat and 175 universal programmer (EG&G Instruments, Princeton, NJ).

*(b) Estimation of Cantilever Spring Constants.* The cantilever spring constant *k* can be estimated theoretically from its dimensions[33] or by several experimental methods. The method of Cleveland et al.[34] measured the change in cantilever resonant frequency with the addition of known end masses to estimate the spring constant. Tungsten spheres were placed upon the cantilever tip and the added mass was plotted against the inverse square of the cantilever resonant frequency, with the slope giving the cantilever spring constant. Here, silica spheres of several different diameters were attached using small, identical droplets of epoxy resin. The mass of the silica sphere and epoxy droplet were evaluated by estimating their volume with an optical microscope and converting to mass via their density. This method gave a spring constant of $k = 0.65 \pm 0.12$ N m$^{-1}$, which is slightly higher than the manufacturer's nominal value of 0.58 N m$^{-1}$. The method of Senden and Ducker,[35] which provides the cantilever spring constant by measuring the normal and inverted cantilever deflection as a function of a known end mass, gave a similar value.

*(c) Force Measurements*. The tip−sample geometry of the AFM force sensing probe is shown in Figure 1b. During the acquisition of a force curve, the measured experimental

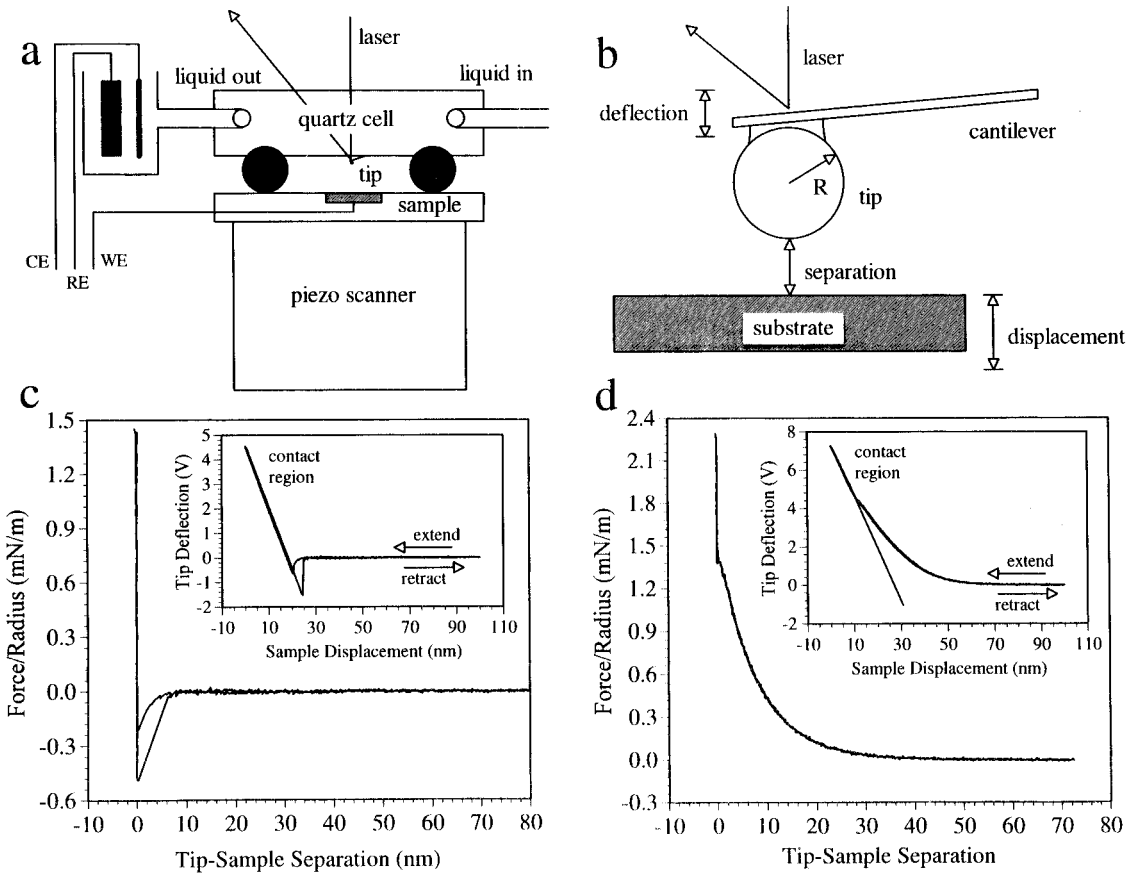


**Figure 1.** (a) Schematic of AFM fluid cell for in situ force and electrochemical measurements. (b) Diagram of modified force-measuring tip and cantilever. (c) Example of force data for attractive tip−sample interaction. The raw data (inset) is converted to a force vs separation format. (d) Example of force data for repulsive tip−sample interaction.

parameters were the cantilever deflection, obtained from the voltage of the sectored photodiode detector, and the substrate displacement, which was given by the piezo scanner voltages. These data were converted to a normalized force (force/radius) vs tip−sample separation for further analysis. Representative force curves for attractive (Figure 1c) and repulsive (Figure 1d) interactions are shown. The raw data (inset), giving the tip deflection vs substrate displacement, are converted to force vs separation with knowledge of the scanner calibration, cantilever spring constant, and tip radius. The tip deflection, which is proportional to the difference signal of the sectored photodiode detector, is calibrated by comparing the detector signal to the piezo displacement in the constant compliance or contact region, which is indicated in the raw data (inset) by the region of linear deflection. The onset of constant compliance is also taken as the point of surface contact. The zero force was found from the static tip deflection at large separations. The data corresponding to the forward (extend) and reverse (retract) scans overlayed quite well except for immediately adjacent to the surface. In the attractive regime (Figure 1c), hysteresis was observed by a larger negative force on the retract curve resulting from tip−sample adhesion. This adhesion force generally decreased as the interaction became repulsive. In many cases (Figure 1d), adhesive forces were absent in purely repulsive regimes.

*(d) Capacitance Measurements*. Differential capacitance curves for gold were generated using a CH Instruments electrochemical workstation (CH Instruments, Memphis, TN) with the ac voltammetry algorithm. The ac frequency was 80 Hz with a peak-to-peak amplitude of 5 mV. The dc potential was scanned at a rate of 10 mV/s from positive to negative potentials in $10^{-3}$ M solutions of KI, KBr, KCl, and NaF. The working electrode consisted of a gold disk in glass with the same exposed area as that used in the AFM cell. This electrode was pretreated in the same manner as that for the AFM measurements. The reference and counter electrodes were the same as cited earlier.

## Results and Discussion

**Theory.** Theories describing the forces between interacting electrostatic double layers have been considered by numerous authors. The interaction between similarly charged double layers at low surface potentials is described by the theory of Derjaguin−Landau−Verwey−Overbeek (DLVO).[36] According to DLVO theory, the total interaction energy between two plates can be considered as the sum of several contributions, including an attractive van der Waals component ($V_A$) and an electrostatic repulsion or attraction ($V_E$). There is also considerable evidence for an additional repulsion ($V_S$) at close separations resulting from the presence of ordered solvent layers.[3a,4b,7b,17]

Using the Derjaguin approximation,[37] the force between spheres of effective radius $R_T$ can be related to the energy between plates by the expression

$$F/R_T = 2\pi(V_A + V_E + V_S) \quad (1)$$

The van der Waals energy ($V_A$) in the nonretarded limit[38,39] is described by an equation of the form

$$V_A = -A_H/12\pi d^2 \quad (2)$$

where $A_H$ is the Hamaker constant and $d$ is the separation distance. The electrostatic interaction ($V_E$) can be derived by considering the free energy associated with the formation of a

double layer[36d,40] or by integrating the electrostatic force.[36d,41] Using the latter method, the interaction for a 1:1 electrolyte is

$$V_E = -\int_{\infty}^{D}\left\{2n^0kT\left[\cosh\left(\frac{ze\psi}{kT}\right)-1\right]-\frac{\epsilon}{2}\left(\frac{d\psi}{dz}\right)^2\right\}dz \quad (3)$$

where $\psi$ is the electrostatic potential. The first term in eq 3 is a repulsive osmotic component that results from the accumulation of charge in the gap between the plates, and the second is a Maxwellian stress that represents an induced charge and is always attractive. For similarly charged surfaces, the second term disappears, leaving a result equivalent to DLVO. To determine $V_E$ explicitly, the electrostatic potential must be known. This can be found by solving the Poisson−Boltzmann equation

$$\frac{d^2\psi}{dz^2} = -\frac{1}{\epsilon_0\epsilon_r}\sum_i n_i^0 z_i e \exp\left(-\frac{z_i e\psi}{kT}\right) \quad (4)$$

Approximations to eq 4 have been solved analytically for several limiting cases.[40,42] Generally, however, the complete nonlinear form of eq 4 must be solved, which can be accomplished only by numerical techniques.[43] In this work, the complete nonlinear form of eq 4 was solved using a finite element discretization of eq 4 with linear basis functions. Integration of eq 3 was then achieved with a Simpsons' 3/8 rule. Details of this calculation are provided in the supporting information. The additional repulsive force ($V_S$) in eq 1 is thought to arise from the presence of ordered solvent layers and can be described by a decaying oscillatory force.[9a] The nature of this repulsive force is not clearly understood and will be neglected in the calculations presented here.

**Limitations of a Passive Cantilever.** The passive cantilever used to measure forces with the standard AFM and with the SFA is limited by the nature of the cantilever. In the presence of purely repulsive forces, the cantilever deflection provides the complete interaction up to surface contact. For attractive interactions, however, the cantilever is limited to forces below a critical snap-in force.[3a,4b] Because the cantilever is a passive and thereby unstable device, attractive forces which exceed a maximum value lead to a critical instability. This instability is characterized by a condition in which the force derivative exceeds the spring constant of the cantilever tip by

$$dF/dD \geq k_s \quad (5)$$

At small surface separations, attractive forces between tip and sample may exceed this value and cause the tip to snap to the surface prior to contact. For purely attractive van der Waals interactions, as exist for the interaction between two uncharged surfaces, the tip−sample force is described by

$$F/R_T = -A_H/6d^2 \quad (6)$$

By substituting this expression into eq 5, the critical snap-in force occurs at

$$d_{snap} = (A_H R_T/3k_s)^{1/3} \quad (7)$$

Thus, the snap-in distance $d_{snap}$ is a function of the Hamaker constant $A_H$, tip radius $R_T$, and cantilever spring constant $k_s$. For $R_T = 6.25\ \mu$m, $A_H = 1.5 \times 10^{-20}$ J, and $k_s = 0.65$ N m$^{-1}$, $d_{snap}$ is 7.8 nm. In the presence of purely van der Waals interactions, $d_{snap}$ gives an independent measure of $A_H$, provided the tip radius and cantilever spring constant are known. However, this phenomenon also prevents accurate measurement of forces existing at separations of less than $d_{snap}$.

**Force Measurements.** The interaction between silica surfaces has been examined by several authors.[10b,13a,b] This interaction was also investigated in this work to determine the silica surface potential under conditions similar to those found while probing the double layer at a gold electrode. Under the conditions examined here, where the solution pH (~5.5) exceeds the isoelectric point ($i_{ep} \approx 2.0$), the silica surface is negatively charged and the silica−silica interaction is purely repulsive. Force−distance curves measured for the silica−silica interaction exhibit an exponential dependence with distance that is well-reproduced by standard DLVO theory.[44] These data, when fit to the sum of repulsive electrostatic and attractive van der Waals interactions, with $A_H = 0.88 \times 10^{-20}$ J,[10b,41,45] provide the surface potential $\psi$ and Debye length $\kappa^{-1}$, where the Debye length is defined by

$$\kappa^{-1} = \sqrt{\frac{\epsilon kT}{4\pi\sum_i n_i e_i^2}} = \frac{0.3045}{\sqrt{C}} \quad (8)$$

In a $10^{-3}$ M KCl solution, a best fit of the data gives a silica surface potential of $\psi = -41$ mV and a Debye length of $\kappa^{-1} = 10.8$ nm. Data at other electrolyte concentrations indicated an increase in the magnitude of the effective surface potential with decreasing concentration. The fitted surface potentials have values similar to those found by other authors with force measurements.[13a,46]

To model the interaction between silica and gold in aqueous solutions, $A_H$ must be determined. Values for this constant have been determined for both the silica−silica[13a,46] and gold−gold[47] interactions. Reported values for silica−silica in aqueous solutions fall in the range of $A_H = 0.88 \times 10^{-20}$ to $2.2 \times 10^{-20}$ J, while $A_H$ for two gold surfaces in an aqueous solution is in the range $25 \times 10^{-20}$−$40 \times 10^{-20}$ J. For the silica−gold interaction, a geometric mean of these values is $A_H = 4.7 \times 10^{-20}$−$9.4 \times 10^{-20}$ J. This can be compared to experimentally measured values. In Figure 2, the purely attractive interaction between silica and gold in air (Figure 2a) and in deionized water (Figure 2b) are depicted, with a best fit to the parabolic, nonretarded van der Waals interaction (eq 2 or 6). For the silica−gold interaction in air, a best fit to this parabolic curve gives $A_H = 2.2 \times 10^{-20}$ J. This can be compared to the value determined by the snap-in distance (eq 7), which occurs at 5.1 nm, and gives a slightly higher Hamaker constant of $A_H = 4.1 \times 10^{-20}$ J. The difference in these values is probably the result of the lower accuracy of the measured snap-in distance, which is limited by the rate of data sampling in the force curve. The Hamaker constant in water is considerably higher than this value. The increase in $A_H$ in aqueous media is due, primarily, to the increase in the dielectric constant (78 vs 1.0).[48] A best fit of the nonretarded van der Waals interaction in purified water (Figure 2b) gives a value of $A_H = 1.2 \times 10^{-19}$ J; the $A_H$ value determined from the snap-in distance of 7.8 nm was $1.5 \times 10^{-19}$ J.

When determining the Hamaker constant in water, the influence of electrostatic forces between silica and gold cannot be completely eliminated. The silica surface is negatively charged under the solution pH conditions (vide supra). The gold surface is maintained at a potential determined by solution composition, i.e., the presence of any specifically adsorbed electrolyte species. At open circuit, the potential should be near the pzc. However, any positive or negative deviations in potential would produce a charge at the electrode

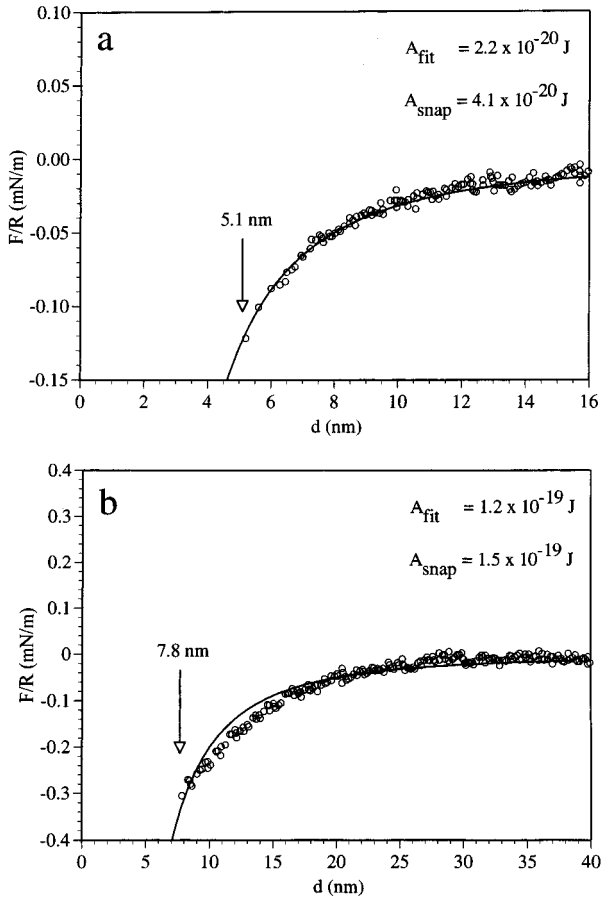


**Figure 2.** Force between silica sphere and gold plate in (a) air and (b) deionized water at 25 °C and pH ≈ 5.5. Attractive force is fit to van der Waals attraction of $F/R = -A_H/6d^2$ and the snap-in distance to $d_{snap} = (A_H R_T/3k_s)^{1/3}$. In air, the silica−gold interaction gave $A_H = 2.2 \times 10^{-20}$ and $4.1 \times 10^{-20}$ J using the curve fit and snap-in distance, respectively. In aqueous solutions, $A_H$ increased to $1.2 \times 10^{-19}$ and $1.5 \times 10^{-19}$ J using these two methods.

and introduces an error in this estimation of $A_H$. Also, the presence of charge at the silica probe can induce an image charge at the gold electrode as the two surfaces approach. The silica−gold interaction was always attractive under open-circuit conditions, suggesting that the gold was either uncharged or slightly positively charged under these conditions. In the latter case, the measured value for $A_H$ would be slightly overestimated.

In the presence of an electrolyte solution with the gold electrode under electrochemical control, the silica−gold interaction is a strong function of the applied potential and the nature of the electrolyte. In aqueous solutions containing KCl, the force vs distance and force vs potential curves depicted in Figure 3 are obtained. In this example, the force between silica and gold as a function of electrode potential in $10^{-3}$ M (Figure 3) and $10^{-2}$ M KCl (Figure 3 inset) are shown. In both systems, the interaction force is seen to be purely repulsive at negative potentials, indicating that the electrode surface is negatively charged, while attractive forces are observed when the electrode is made positive. In $10^{-3}$ M solutions, the force vs distance interaction extends past 30-nm separation, while in $10^{-2}$ M solutions, the interaction force decays within the first 8 nm from the electrode surface. This behavior is consistent with the difference in the calculated Debye screening length for these solutions, $\kappa^{-1} = 9.62$ nm at $10^{-3}$ M and $\kappa^{-1} = 3.04$ nm at $10^{-2}$ M. However, in both, the shape of the decay in force with distance is the same as is the dependence with electrode potential.

The change in force with potential between the negative silica tip and the gold electrode is readily understood in terms of the nature of the double layer at the gold electrode.[49] The silica tip probes the diffuse double layer (dl) near the electrode surface. This consists of counterions that balance the charge injected into the gold electrode (and residing at the gold/solution interface) and the charge from any specifically adsorbed ions (e.g., $Cl^-$) on the electrode surface (at the inner Helmholtz plane). At the pzc, the charge from the adsorbed $Cl^-$ is totally compensated by positive charge on the gold, so that no diffuse dl forms. When the potential of the electrode is made more negative, the net electrode charge becomes negative and a diffuse dl with a net positive charge forms by increasing the local concentration of $K^+$ and decreasing the local concentration of $Cl^-$. The $K^+$ ions are thought to be nonspecifically adsorbed because of a strongly bound solvent shell. Under these conditions, the force between the negatively charged silica probe ($\psi_p = -41$ mV), with its positively charged diffuse dl, and the gold is repulsive, as seen in the upper curves in Figure 3. At sufficiently negative potentials, the specifically adsorbed $Cl^-$ is removed from the surface, so the net surface charge is that of the gold. When the potential of the electrode is made more positive, the net surface charge becomes positive and the diffuse dl forms by repulsion of $K^+$ and attraction of $Cl^-$. The negative potential drop through this dl produces an attractive force between the silica probe and the electrode (lower curves in Figure 3).

A theoretical treatment of the potential dependence of this interaction can be produced by solving for the potential distribution via the nonlinear Poisson−Boltzmann equation and thus the interaction force (vide supra). Figure 4 depicts a representative calculation for the force between a sphere and plate, with the force scaled to the probe radius. These values can be converted to the interaction energy between two plates by dividing the force by $2\pi$. These calculations include both electrostatic and van der Waals interactions, with $A_H = 1.2 \times 10^{-20}$ J and $\kappa^{-1} = 9.62$ nm. With boundary conditions constrained to a constant surface potential at both the probe and substrate, the behavior depicted by Figure 4a is obtained. The curves represent a fixed surface potential of $\psi_p = -41$ mV at the probe and potentials ranging from $\psi_s = -100$ to 100 mV at the substrate. The upper curve corresponds to $\psi_p = -41$ and $\psi_s = -100$ mV and the lower corresponds to $\psi_p = -41$ and $\psi_s = 100$ mV. When the probe and substrate have potentials of opposite sign, the force is purely attractive (lower curve). When the two surfaces have potentials of the same sign, the interaction is repulsive at large separations and becomes attractive as the surfaces approach (upper curve). This leads to a maximum in the force−distance curve. The presence of this maximum is due both to the onset of attractive van der Waals interactions and also from the nature of the boundary conditions. At constant potential, the charge on both surfaces may change. When the surfaces have a potential of the same sign, the charge on the surface with the smaller potential will change sign as the surfaces approach because of an induced charge from the surface of higher potential, which leads to an attractive force. For surfaces with potentials of opposite sign, the surface charges will both increase in magnitude as the surfaces approach, which leads to an even larger attractive force. Both effects can be seen as an image charge effect that increases the influence of the Maxwellian stress term in eq 3 at close separations.

When the surfaces are maintained at a constant surface charge, the behavior depicted in Figure 4b is observed, where the surface potentials at infinite separation are the same as those in Figure

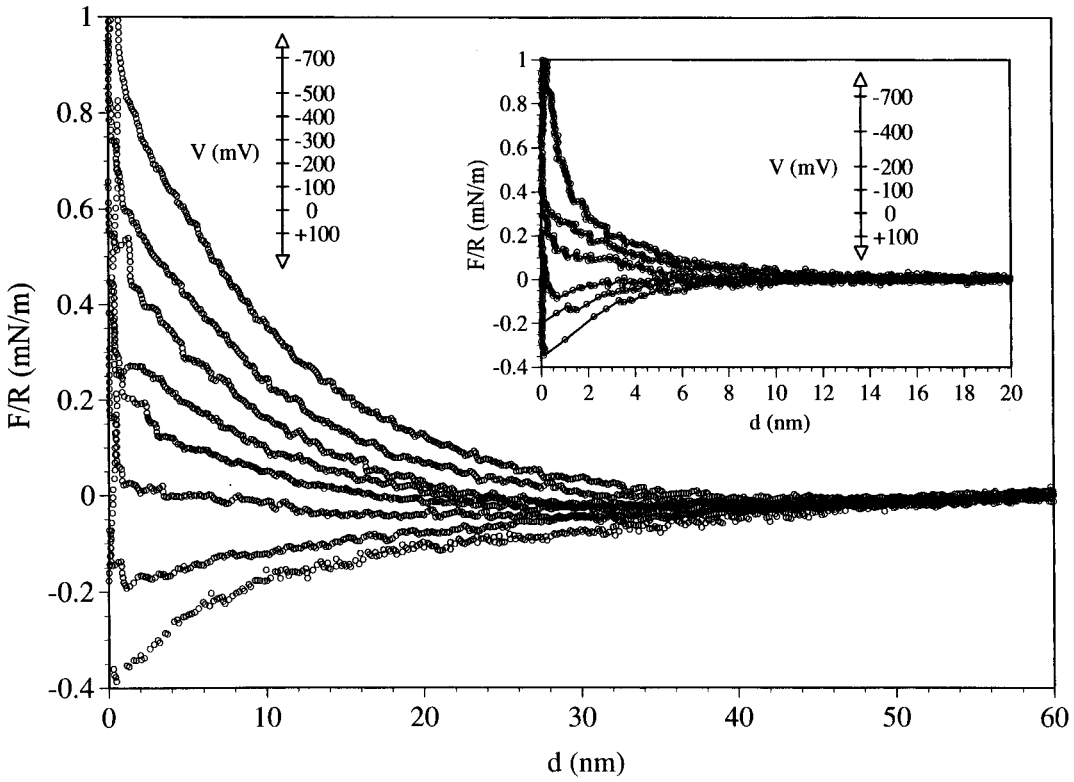


**Figure 3.** Force between silica sphere and gold electrode in an aqueous solution of $10^{-3}$ M KCl at 25 °C and pH ≈ 5.5 as a function of the applied potential at gold electrode. The curves correspond to, from top to bottom, electrode potentials of −700, −500, −400, −300, −200, −100, 0, and 100 mV (vs SCE). Electrostatic repulsion decreases as the electrode potential increases from −700 to 100 mV. Inset: force data for silica sphere and gold substrate in $10^{-2}$ M KCl solution.

4a. Under these conditions, the interaction is more repulsive than when the surfaces are maintained at constant potential. At a fixed surface charge, the Maxwellian stress term remains constant, but the osmotic pressure increases as the surfaces approach because of the electroneutrality requirement, as dictated by the Poisson−Boltzmann equation. This requirement forces the potential on both surfaces to increase to more positive values to maintain a constant surface charge as the separation distance decreases. Although a maximum in the force curves in Figure 4b is seen, this is solely the result of the attractive van der Waals contribution that emerges at close separations.

The behavior corresponding to constant potential and constant surface charge boundary condition has been compared to experimental measurements in a variety of systems. Generally, constant surface charge boundary conditions more accurately reflect experimental data. However, both models diverge from experimental results at small surface separations. In the absence of van der Waals interactions, the theoretical data for constant charge tends to overestimate the measured force, while constant potential underestimates this value. Both models underestimate the observed force at separations of less than 5−10 nm, particularly when a van der Waals interaction is included in the theory. This deviation is likely a result of the additional repulsive force due to solvent ordering.[3a,4b,7b,17]

When experimental force data at selected electrode potentials for the silica−gold system in $10^{-3}$ M KCl solutions (Figure 3) are fit to theoretical curves, the results in Figure 5 are obtained. The electrode potentials correspond to −700 mV (Figure 5a), −300 mV (Figure 5b), −100 mV (Figure 5c), and 100 mV (Figure 5d). The model results (solid curves) represent a best fit to the data (open circles) at distances of 10 nm and greater using $\kappa^{-1} = 9.62$ nm, corresponding to a $10^{-3}$ M solution. The upper curve (thick line) is for the model at constant surface charge, while the lower (thin line) is at constant surface potential.

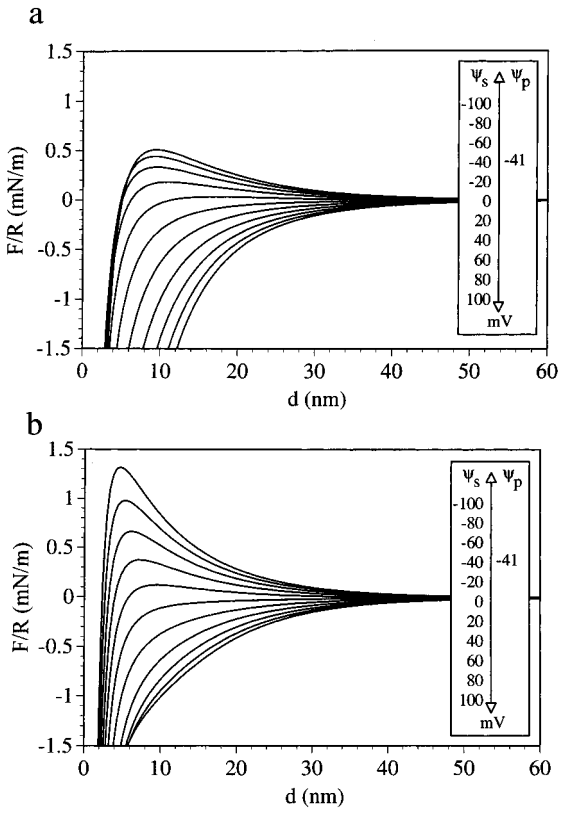


**Figure 4.** Calculated force between dissimilar sphere and plate as a function of plate potential in $10^{-3}$ M aqueous solution of 1:1 electrolyte using numerical solution to nonlinear Poisson−Boltzmann equation and nonretarded Hamaker constant of $1.2 \times 10^{-19}$ J. The curves show (a) constant surface potential and (b) constant surface charge boundary conditions with the potential of the sphere held at $\psi_p = -41$ mV and the potential of the plate varied from $\psi_s = -100$ to 100 mV.

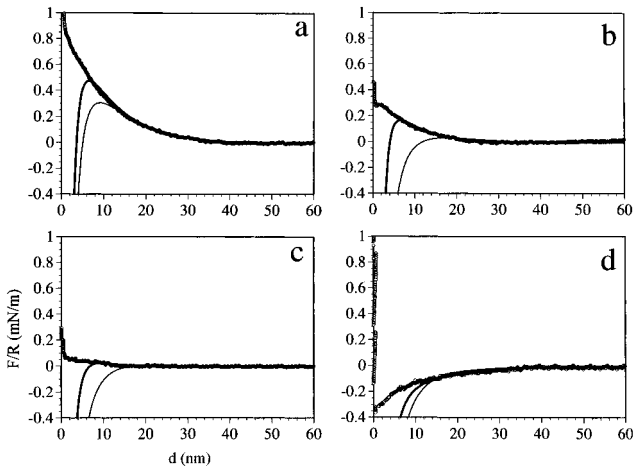


**Figure 5.** Measured and theoretical force between silica sphere and gold substrate at constant charge (thick line) and constant potential (thin line) in an aqueous $10^{-3}$ M KCl solution at 25 °C and pH ≈ 5.5. In each fit, the silica surface at infinite separation is maintained at $\psi_p = -41$ mV, $A_H = 1.2 \times 10^{-19}$ J, and $\kappa^{-1} = 9.62$ nm. $\psi_s{}^{\sigma}$ = constant charge and $\psi_s{}^{\psi}$ = constant potential: (a) $E = -700$ mV (vs SCE): $\psi_s{}^{\sigma} = -47$ mV, $\psi_s{}^{\psi} = -55$ mV; (b) $E = -300$ mV (vs SCE): $\psi_s{}^{\sigma} = -22$ mV, $\psi_s{}^{\psi} = -25$ mV; (c) $E = -100$ mV (vs SCE): $\psi_s{}^{\sigma} = -7$ mV, $\psi_s{}^{\psi} = -12$ mV; (d) $E = 100$ mV (vs SCE): $\psi_s{}^{\sigma} = 5$ mV, $\psi_s{}^{\psi} = -2$ mV. The data points are depicted by circles while the theoretical curves are solid lines.

The surface potential at infinite separation is set at a value giving the best fit in each case. The theoretical models diverge severely from the measured data at separations of less than 10 nm. This is likely the result of several factors. First, an overestimate of $A_H$ would lower the theoretical force at small separations. As the influence of attractive electrostatic forces in the measurement of $A_H$ could not be eliminated, an overestimate of $A_H$ is likely. Second, the plane of surface charge may lie negative of the onset of surface contact. The nontrivial roughness of the silica probe and gold substrate would lead to contact between probe and sample that is positive of the mean surface plane. In each data set, a better fit is obtained with the plane of surface charge moved 3−5 nm negative of the contact position. Also, a solvent repulsion term was not included in the theoretical curves and would improve the fit to data. Nevertheless, in each example, the condition of constant surface charge more closely reflects the experimental data. In Figure 5a, which is for an applied potential of −700 mV (vs SCE), a purely repulsive interaction is observed. The best fit to these data, with the silica surface kept at a constant potential of $\psi_p = -41$ mV, can be obtained with the parameters $\psi_s{}^{\sigma} = -47$ mV at constant charge and $\psi_s{}^{\psi} = -55$ mV at constant potential. As the electrode potential is increased to more positive values, the forces transform from repulsive to attractive. The other data gives best fit parameters to the theoretical curves of −300 mV, $\psi_s{}^{\sigma} = -22$ mV and $\psi_s{}^{\psi} = -25$ mV; −100 mV, $\psi_s{}^{\sigma} = -7$ mV and $\psi_s{}^{\psi} = -12$ mV; and 100 mV, $\psi_s{}^{\sigma} = +5$ mV and $\psi_s{}^{\psi} = -2$ mV.

**Determination of PZC.** Regardless of the boundary conditions employed in the theoretical models, the force−distance curves more accurately reflect the data as the separation between surfaces increases. At larger separations, where the influence of van der Waals and solvent interactions is negligible, the measured force decreases monotonically from repulsive to attractive as the electrode potential is increased from negative to positive values. In the model curves (Figure 4), this change in force from repulsive to attractive reflects a change in the surface potential (or charge) of the electrode from negative to positive values. Thus, at larger separations, a change in electrode potential that decreases the force from repulsive to attractive should reflect a surface potential at which the charge is zero, corresponding to the pzc.

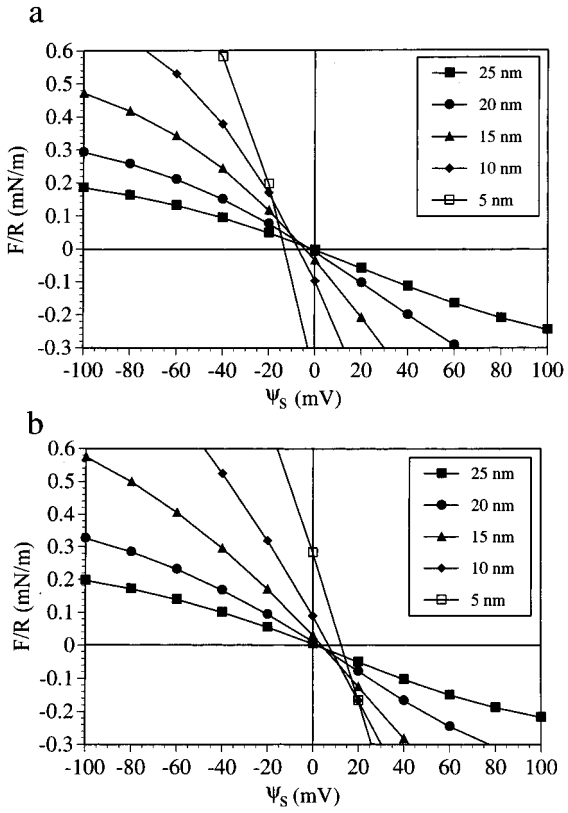


**Figure 6.** Theoretical electrostatic force, in absence of attractive van der Waals interactions, as determined by numerical solution to nonlinear Poisson−Boltzmann equation at fixed separations of 5, 10, 15, 20, and 25 nm between sphere held at surface potential of −41 mV and plate in $10^{-3}$ M solution as a function of the plate potential: (a) predicted force at constant potential conditions and (b) predicted force at constant charge conditions.

In Figure 6, the theoretical data corresponding to the electrostatic component of the force at both constant surface potential and constant charge boundary conditions are plotted as force vs surface potential at several fixed separations. The force−potential curves are approximately linear through the pzc at each separation, but reach a plateau as the surface potential increases to large positive or negative values. With a constant surface potential boundary condition (Figure 6a), the force directly adjacent to the electrode surface ($d = 5$ nm) achieves a value of zero that is negative of the pzc. However, as the distance between electrode and probe is increased, the potential of zero force (pzf) converges to the pzc. A similar behavior occurs when the surface charge is kept constant in the model (Figure 6b). In this case, however, zero force occurs at a potential exceeding the pzc when the force is measured near the electrode surface but, again, converges to the pzc at larger separations. In each model, the pzc and pzf converge to the same value at separations of greater than 15 nm for a $10^{-3}$ M electrolyte.

When the experimentally measured force for a $10^{-3}$ M KCl solution is plotted at several fixed separations as a function of the electrode potential, the curves in Figure 7 are seen. The shape of these curves is similar to that observed in Figure 6 for the theoretical results, exhibiting a linear decrease from repulsive to attractive forces as the potential is increased from negative to positive values. The forces also begin to plateau at potentials far positive and negative of that corresponding to the zero force. At positive potentials, the force is nearly constant with potential at a fixed separation. This constancy of the attractive force is

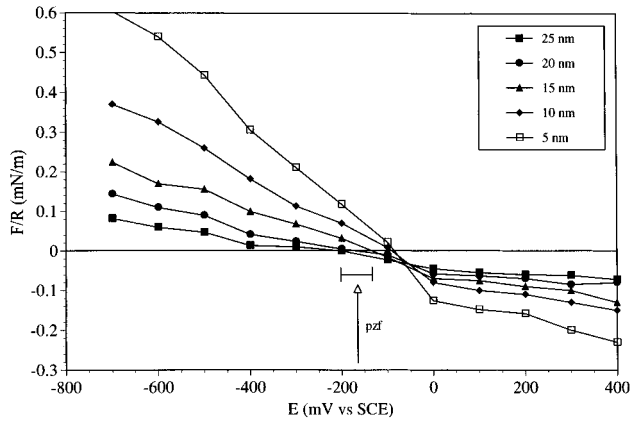


**Figure 7.** Force between silica sphere and gold electrode in $10^{-3}$ M KCl solution at fixed separations of 5, 10, 15, 20, and 25 nm as a function of electrode potential. The potential of zero force (pzf) is shown.

due to the snap-in of the cantilever and illustrates the major inadequacy of passive cantilever probes. When the force becomes purely attractive, it exceeds the critical snap-in force determined by the cantilever spring constant. Typically, attractive forces near a surface are inaccessible.

As seen in the theory for constant surface charge (Figure 6b), the measured pzf generally decreases as the probe−electrode separation increases. This would suggest that the constant charge model more accurately reflects experimental observations than the constant surface potential model. This was also observed when fitting the complete force vs distance curves (see Figure 5). In the limit of large probe−electrode separations, corresponding to distances greater than 15 nm in Figure 7, the pzf occurs at an electrode potential of approximately −150 mV (vs SCE) in KCl solutions. The measured pzf varied by approximately ±75 mV when different gold substrates and tips were used.

The pzc of an electrode depends upon the nature of the electrolyte, particularly the extent of specific adsorption of the anions. As the strength of anion adsorption increases, the pzc shifts to more negative values. This has been observed for the series $F^-$, $Cl^-$, $Br^-$, and $I^-$ on mercury and gold electrodes,[31a,b] where the pzc is most positive for $F^-$ and decreases to more negative values, with $I^-$ exhibiting the most negative pzc. Generally, the nature of the alkali metal cation has a much smaller influence on the pzc, since these generally do not specifically adsorb.

An early study of the interaction between two similar metal wires as a function of electrode potential showed a minimum near the pzc.[2] Measurement of the force between a negatively charged silica probe and a gold electrode surface in KCl solutions indicates a variation where positive electrode potentials provide for an attractive force while excursions toward negative potentials introduce a repulsive force. Similar variations are also observed for a gold electrode in the presence of other simple 1:1 electrolytes, mainly NaF, KBr, and KI. Figure 8 illustrates the force−distance curves for all four systems as a function of electrode potential in $10^{-3}$ M solutions. In each case the force is attractive at positive potentials. At negative potentials, the interaction force transforms to a purely repulsive interaction. The shape of the force vs distance curves in these systems is similar at larger separations, indicating a comparable Debye length. At small probe−substrate separation, the curves differ somewhat, with definite maxima appearing in several measurements (Figure 8a,c). The presence of these maxima suggest improved probe−substrate contact, as predicted by theoretical models.

The pzf in these systems, much as the pzc, varies with the nature of the electrolyte. Plotting the force vs potential at a separation of 15 nm for KI, KBr, KCl, and NaF, results in the curves in Figure 9a. The shape of these curves is similar for each electrolyte, but with a different pzf. For NaF, the pzf occurs in the potential range 0 to +400 mV. The pzf for NaF shifted within this range with the history of the electrode. In KCl solutions, the pzf occurred at −150 mV. In KBr, the pzf was at even more negative potentials, typically in the range −250 to −350 mV, while KI solutions exhibited the most negative pzf, between −600 and −650 mV.

These results indicate that the process responsible for the shape of the force curves is similar in each electrolyte, while the potential dependence is a strong function of the solution composition. The nature of the anion plays a strong role in determining the potential at which the double-layer force approaches a value of zero. Theoretical models of the double-layer interaction indicate that this minimum in force converges to the pzc at separations of greater than 15 nm.

A number of methods have been proposed for determining the pzc of solid metal electrodes. Frequently, this is found from the electrode capacitance, as measured by ac voltammetry or impedance methods.[49] The theoretical form of the diffuse layer capacitance is given by

$$C_{\mathrm{dif}} = \epsilon\epsilon_0\kappa \cosh[ze(\psi - \psi_{\mathrm{pzc}})/2kT] \qquad (9)$$

The minimum in the double-layer capacitance occurs at a potential $\psi$ corresponding to the pzc, $\psi_{\mathrm{pzc}}$. The pzc of several electrode materials, including gold and mercury, has been examined by ac voltammetric methods.[31a,b] The response of a gold electrode surface identical with that examined in the AFM fluid cell is shown in the capacitance curves in Figure 9b. The four electrolyte solutions exhibit electrode capacitance values ranging from approximately 5 to 15 $\mu$F cm$^{-2}$. Each encounters a minimum in this capacitance. These minima occur at KI, −640 mV; KBr, −250 mV; KCl, −100 mV; and NaF, 225 mV. The potential of minimum capacitance was quite reproducible (±50 mV) for KI, KBr, and KCl, with only a slight variation with different electrode samples. However, the potential for NaF varied over the range 0 to +400 mV (vs SCE). A variation in the pzc of gold electrodes in $F^-$ solutions has been observed and is said to be related to the crystallinity of the electrode[50] but may also be caused by adsorption of organic impurities which also depress the capacitance.[49]

The potentials corresponding to values of the minimum in electrode capacitance agree quite well with the potentials of minimum force on the same electrode surface. In each system, the pzc measured by ac voltammetry is within the error bars of the pzf determined by force measurements. This correlation between force and charge is supported by the theoretical calculations, which indicate that the force between two surfaces should pass through a minimum at the pzc as the separation distance increases, regardless of the boundary conditions employed in the model. At smaller surface separations, the influence of attractive van der Waals interactions and solvent forces obscure the purely electrostatic forces.

## Conclusions

The forces between a silica probe and either silica or gold substrates were measured using an AFM in the presence of a series of alkali halide electrolyte solutions. The silica−silica interaction was repulsive and accurately predicted by standard DLVO theory except at very small separations, where an additional repulsion was observed. The silica surface was

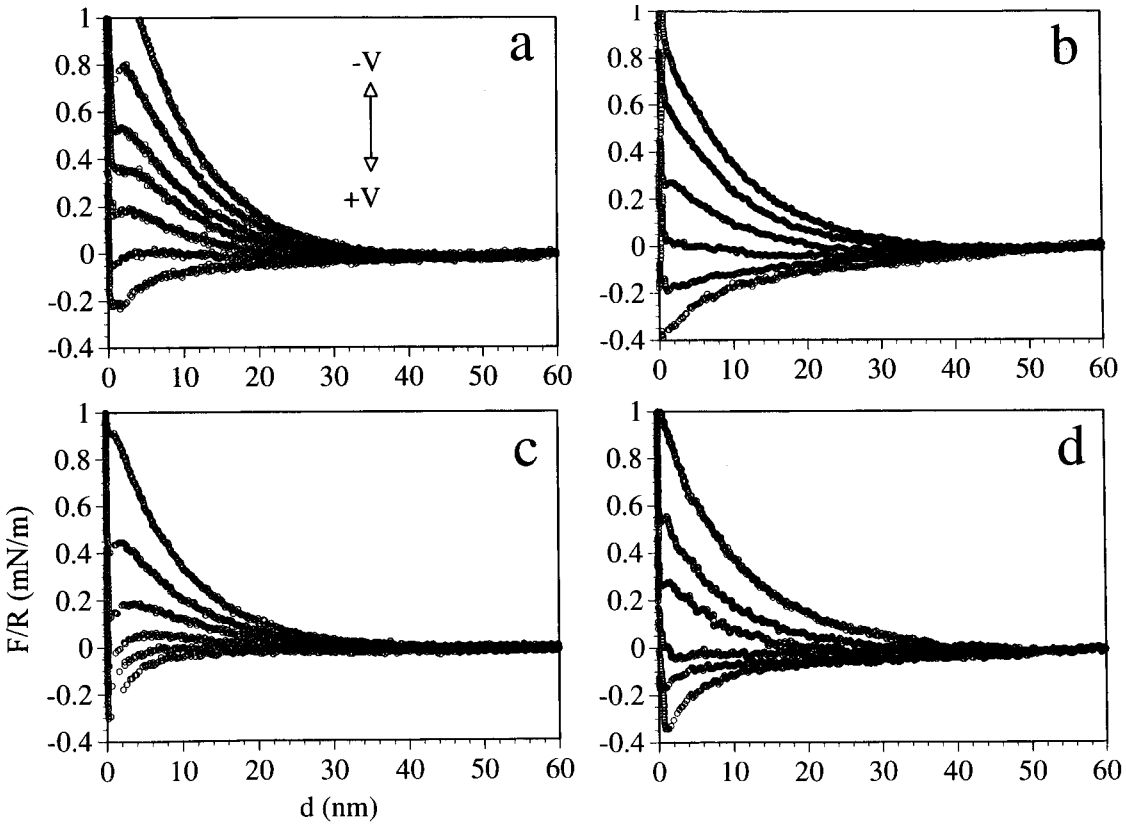


**Figure 8.** Force between silica sphere and gold substrate as a function of electrode potential in $10^{-3}$ M aqueous solutions of (a) NaF, (b) KCl, (c) KBr, and (d) KI. The curves correspond to, from top to bottom, electrode potentials of (a) −600, −400, 0, 200, 300, 400, and 600 mV; (b) −700, −500, −300, −100, 0, and 100 mV; (c) −600, −500, −400, −300, −200, and −100 mV; (d) −900, −800, −700, −600, −500, and −400 mV (vs SCE). Electrostatic repulsion decreases as the electrode potential increases from negative to positive potentials.

negatively charged at a pH of 5.5 and a fit to DLVO theory gave a surface potential of −41 mV in $10^{-3}$ M KCl with a Debye length of $\kappa^{-1} = 10.8$ nm, comparable to the value determined from the solution concentration of $\kappa^{-1} = 9.62$ nm. The interaction between silica and gold surfaces, in contrast, exhibited an attractive interaction at neutral pH. Under electrochemical conditions, the silica−gold interaction was a strong function of the potential applied to the gold electrode and also the nature of the electrolyte species. The silica−gold interaction was attractive at positive potentials and repulsive at negative potentials. A series of force measurements obtained as a function of the potential of the gold electrode indicates that the effective surface potential (and charge) of the gold electrode decreases while moving from positive to negative potentials, corresponding to the removal of adsorbed anions from the electrode surface. The potential at which the silica−gold force passes through a minimum corresponds closely to the pzc in solutions of NaF, KCl, KBr, and KI. The pzf values determined from force measurements are quite similar to pzc values determined from electrode capacitance measurements. Theoretical fits of the force data to solutions of the complete nonlinear Poisson−Boltzmann equation indicate that although the constant surface charge most accurately reflects the data, neither constant surface potential or charge boundary conditions fit the data at small surface separations. This poor fit at small separations is attributed to an overestimate of the Hamaker constant, an ill-defined location for the plane of surface charge, and the presence of short-range repulsive solvent forces. However, the models converge toward the experimental behavior as the distance from the electrode increases. A comparison of the theoretical and experimental data indicates that the pzf corresponds to the pzc at separations greater than approximately 15 nm in $10^{-3}$ M solution.

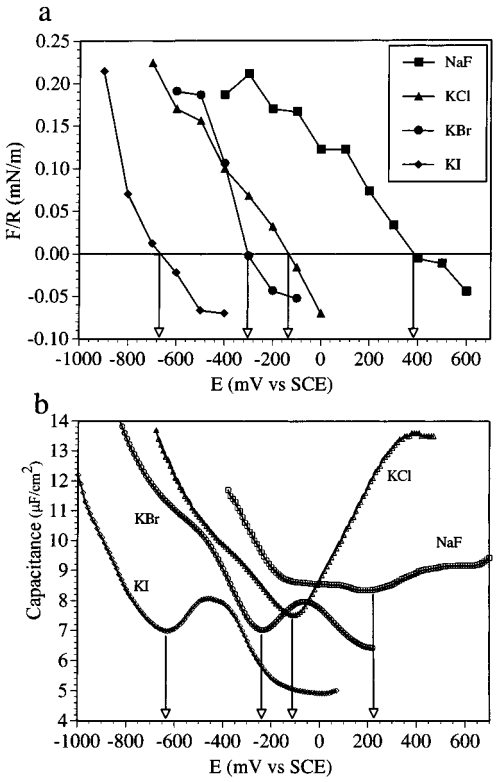


**Figure 9.** (a) Force between silica sphere and gold electrode at a separation of 15 nm in $10^{-3}$ M solutions of KI, KBr, KCl, and NaF as a function of electrode potential. The potential of zero force is indicated by arrows. (b) Differential capacitance of gold electrode in $10^{-3}$ M aqueous solutions of KI, KBr, KCl, and NaF. The minimum in differential capacitance, corresponding to the potential of zero charge, is indicated by an arrow in each curve.

These studies indicate the utility of force measurements in characterizing the properties of the electrode/electrolyte interface. They provide for an alternative measurement of the pzc, as well as for the examination of related surface forces, including solvent ordering and solute adsorption at electrodes.

**Acknowledgment.** The support of this research by the Robert A. Welch Foundation is gratefully acknowledged.

**Supporting Information Available:** Numerical solution to the nonlinear Poisson−Boltmann equation and details of the force measurements between silica probe and substrate (3 pages). See any current masthead page for ordering information and Internet access instructions.

## References and Notes

(1) (a) Derjaguin, B. V.; Rabinovich, Y. I.; Churaev, N. V. *Nature* **1978**, *272*, 313. (b) Israelachvili, J. N. *Intermolecular and Surface Forces*, 2nd ed.; Academic Press: New York, 1991.

(2) Derjaguin, B. V.; Voropayeva, T. N.; Kabanov, B. N.; Titiyevskaya, A. S. *J. Colloid Sci.* **1964**, *19*, 113.

(3) (a) Israelachvili, J. N.; Adams, G. E. *J. Chem. Soc., Faraday Trans. 1* **1978**, *74*, 975. (b) Parker, J. L.; Christenson, H. K.; Ninham, B. W. *Rev. Sci. Instrum.* **1989**, *60*, 3135.

(4) (a) Horn, R. G.; Israelachvili, J. N. *J. Chem. Phys.* **1981**, *75*, 1400. (b) Shubin, V; Kekicheff, P. *J. Colloid Interface Sci.* **1993**, *155*, 108. (c) Crassous, J.; Elisabeth C.; Gayvallet, H.; Loubet, J.-L. *Langmuir* **1993**, *9*, 1995.

(5) (a) Klein, J. *Adv. Colloid Interface Sci.* **1982**, *16*, 101. (b) Klein, J. *Nature* **1980**, *288*, 240. (c) Israelachvili, J. N. *Macromolecules* **1984**, *17*, 204. (d) Marra, J.; Hair, M. L. *J. Phys. Chem.* **1988**, *92*, 6044.

(6) Christenson, H. K.; Horn, R. G.; Israelachvili, J. N. *J. Colloid Interface Sci.* **1982**, *88*, 79.

(7) (a) Chan, D. Y. C.; Horn, R. G. *J. Chem. Phys.* **1985**, *83*, 5311. (b) Parker, J. L.; Christenson, H. K. *J. Chem. Phys.* **1988**, *88*, 8013.

(8) Claesson, P. M.; Parker, J. L.; Froberg, J. C. *J. Dispersion Sci. Technol.* **1994**, *15*(3), 375.

(9) (a) Parker, J. L. *Surf. Sci.* **1994**, *3*, 205. (b) Stewart, A. M.; Parker, J. L. *Rev. Sci. Instrum.* **1992**, *63*, 5626.

(10) (a) Parker, J. L.; Yaminsky, V. V.; Claesson, P. M. *J. Phys. Chem.* **1993**, *91*, 7706. (b) Grabbe, A.; Horn, R. G. *J. Colloid Interface Sci.* **1993**, *157*, 375.

(11) Binnig, G.; Quate, C.; Gerber, G. *Phys. Rev. Lett.* **1986**, *56*, 930.

(12) Binnig, G.; Rohrer, H.; Gerber, C.; Weibel, E. *Phys. Rev. Lett.* **1982**, 49, 57.

(13) (a) Ducker, W. A.; Senden, T. J.; Pashley, R. M. *Langmuir* **1992**, *8*, 1831. (b) Meagher, L.; Pashley, R. M. *Langmuir* **1995**, *11*, 4019. (c) Biggs, S. *Langmuir* **1995**, *11*, 156. (d) Larson, I.; Drummond, C. J.; Chan, D. Y. C.; Grieser, F. *J. Phys. Chem.* **1995**, *99*, 2114. (e) Li, Y. Q.; Tao, N. J.; Pan, J.; Garcia, A. A.; Lindsay, S. M. *Langmuir* **1993**, *9*, 637. (f) Milling, A.; Biggs, S. *J. Colloid Interface Sci.* **1995**, *170*, 604. (g) Atkins, D. T.; Pashley, R. M. *Langmuir* **1993**, *9*, 2232. (h) Rabinovich, Ya. I.; Yoon, R.-H. *Langmuir* **1994**, *10*, 1903. (i) Rutland, M. W.; Senden, T. J. *Langmuir* **1993**, *9*, 412. (j) Karaman, M. E.; Meagher, L.; Pashley, R. M. *Langmuir* **1993**, *9*, 1220.

(14) (a) Lin, X.-Y.; Creuzet, F.; Arribart, H. *J. Phys. Chem.* **1993**, *97*, 7272. (b) Arai, T.; Fujihira, M. *J. Electroanal. Chem.* **1994**, *374*, 269.

(15) (a) Biggs, S.; Mulvaney, P.; Zukoski, C. V.; Grieser, F. *J. Am. Chem. Soc.* **1994**, *116*, 9150. (b) Biggs, S.; Mulvaney, P. *J. Chem. Phys.* **1994**, *100*, 8501.

(16) (a) Ishino, T.; Hieda, H.; Tanaka, K.; Gemma, N. *Jpn. J. Appl. Phys. Part 1* **1994**, *33*, 4718. (b) Ishino, T.; Hieda, H.; Tanaka, K.; Gemma, N. *Jpn. J. Appl. Phys. Part 2* **1994**, *33*, L1552.

(17) O'Shea, S. J.; Welland, M. E.; Pethica, J. B. *Chem. Phys. Lett.* **1994**, *223*, 336.

(18) Thomas, R. C.; Tangyunyong, P.; Houston, J. E.; Michalske, T. A.; Crooks, R. M. *J. Phys. Chem.* **1994**, *98*, 493.

(19) Thomas, R. C.; Houston, J. E.; Crooks, R. M.; Kim. T.; Michalske, T. A. *J. Am. Chem. Soc.* **1995**, *117*, 3830.

(20) (a) Miller, G. L.; Griffith, J. E.; Wagner, E. R.; Grigg, D. A. *Rev. Sci. Instrum.* **1991**, *62*, 705. (b) Grigg, D. A.; Russell, P. E.; Griffith, J. E. *Ultramicroscopy* **1992**, *42*−*44*, 1504.

(21) Joyce, S. A.; Houston, J. E. *Rev. Sci. Instrum.* **1991**, *62*, 710.

(22) Fan, F.-R. F.; Bard, A. J. *J. Am. Chem. Soc.* **1987**, *109*, 6262.

(23) Smith, C. P.; Maeda, M.; Atanososka, L.; White, H. S.; McClure, D. J. *J. Phys. Chem.* **1988**, *92*, 199.

(24) Raiteri, R.; Butt, H.-J. *J. Phys. Chem.* **1995**, *99*, 15728.

(25) (a) Pangarov, N.; Kolarov, G. J. *J. Electroanal. Chem.* **1978**, *91*, 281. (b) Fredlein, R. A.; Damjanovic, A.; Bockris, J. O'M. *Surf. Sci.* **1971**, *25*, 261. (c) Beck, T. R. *Phys. Chem.* **1969**, *75*, 466.

(26) Seo, M.; Ueno, K. *J. Electrochem. Soc.* **1996**, *143*, 899.

(27) (a) Gouy, G. *J. Phys.* **1910**, *4*, 457. (b) Chapman, D. L. *Philos. Mag.* **1913**, *6*, 475. (c) Debye, P.; Huckel, E. *Phys. Z.* **1923**, *24*, 185. (d) Debye, P.; Huckel, E. *Phys. Z.* **1924**, *24*, 97.

(28) (a) Grahame, D. C. *Chem. Rev.* **1947**, *41*, 441. (b) Frumkin, A. N. *J. Electrochem. Soc.* **1960**, *101*, 461. (c) Parsons, R. In *Advances in Electrochemistry and Electrochemical Engineering*; Gerischer, H., Tobias, C. W., Eds.; Wiley-Interscience: New York, 1961; Vol. 1. (d) Delahay, P. *Double Layer and Electrode Kinetics*; Wiley-Interscience: New York, 1965.

(29) Smith, C. P.; White, H. S. *Anal. Chem.* **1992**, *64*, 2398.

(30) Meites, L. *J. Am. Chem. Soc.* **1951**, *73*, 2035.

(31) (a) Clavilier, J.; Nguyen, V. H. *J. Electroanal. Chem.* **1973**, *41*, 193. (b) Tucceri, R. I.; Posadas, D. *J. Electroanal. Chem.* **1985**, *191*, 387. (c) Piela, B.; Wrona, P. K. *J. Electroanal. Chem.* **1995**, *388*, 69.

(32) Jaschke, M.; Butt, H.-J. *Rev. Sci. Instrum.* **1995**, *66*, 1258.

(33) (a) Neumeister, J. M.; Ducker, W. A. *Rev. Sci. Instrum.* **1994**, *65*, 2527. (b) Sader, J. E. *Rev. Sci. Instrum.* **1995**, *66*, 4583.

(34) (a) Cleveland, J. P.; Manne, S.; Bocek, D.; Hansma, P. K. *Rev. Sci. Instrum.* **1993**, *64*, 403. (b) Sader, J. E.; Larson, I.; Mulvaney, P.; White, L. R. *Rev. Sci. Instrum.* **1995**, *66*, 3789.

(35) Senden, T. J.; Ducker, W. *Langmuir* **1994**, *10*, 1003.

(36) (a) Derjaguin, B. *Trans. Faraday Soc.* **1940**, *36*, 203. (b) Derjaguin, B. V.; Landau, L. D. *Acta Phys. Chem.* **1941**, *14*, 633. (c) Derjaguin, B. V.; Landau, L. D. *J. Exp. Theor. Phys.* **1941**, *11*, 802. (d) Verwey, E. J. W.; Overbeek, J. T. G. *Theory of the Stability of Lyophobic Colloids*; Elsevier: New York, 1948.

(37) Derjaguin, B. V. *Kolloid Z.* **1934**, *69*, 155.

(38) Hartmann, U. *Phys. Rev. B* **1991**, *43*, 2404.

(39) (a) Lifshitz, E. M. *Sov. Phys.-JETP* **1956**, *2*, 73. (b) Dzyaloshinskii, I. E.; Lifshitz, E. M.; Pitaevskii, L. P. *Sov. Phys.-JETP* **1960**, *37*, 165.

(40) Hogg, R.; Healy, T. W.; Fuerstenau, D. W. *Trans. Faraday Soc.* **1966**, *62*, 1638.

(41) Hunter, R. J. *Foundations of Colloid Science*; Oxford University Press: Oxford, 1987.

(42) Gregory, J. *J. Colloid Interface Sci.* **1975**, *51*, 44.

(43) (a) Chan, D. Y. C.; Pashley, R. M.; White, L. R. *J. Colloid Interface Sci.* **1980**, *77*, 283. (b) McCormack, D.; Carnie, S. L.; Chan, D. Y. C. *J. Colloid Interface Sci.* **1995**, *169*, 177.

(44) These data are provided in the supporting information.

(45) Hough, D. B.; White, L. R. *Adv. Colloid Interface Sci.* **1980**, *81*, 285.

(46) (a) Horn, R. G.; Smith, D. T.; Haller, W. *Chem. Phys. Lett.* **1989**, *162*, 404. (b) Peschel, G.; Belouschek, P.; Muller, M. M.; Muller, M. R.; Konig, R. *Colloid Polym. Sci.* **1982**, *260*, 444. (c) Rabinovich, Y. I.; Derjaguin, B. V.; Churaev, N. *Adv. Colloid Interface Sci.* **1982**, *16*, 63.

(47) (a) Schrader, M. E. *J. Colloid Interface Sci.* **1984**, *100*, 372. (b) Rabinovich, Ya. I.; Churaev, N. V. *Russ. J. Phys. Chem.* **1990**, *52*, 256.

(48) *Handbook of Chemistry and Physics*, 50th ed.; Weast, R. C., Ed.; The Chemical Rubber Co.: Cleveland, OH, 1970.

(49) Bard, A. J.; Faulkner, L. R. *Electrochemical Methods: Fundamentals and Applications*; John Wiley & Sons: New York, 1980; Chapter 12.

(50) Lecoeur, J.; Sella, C.; Martin, J. C.; Tertian, L.; Deschamps. H. *C. R. Acad. Sci.* **1975**, *281C*, 71.

JP961629K